Applied Surface Science 307 (2014) 234–240

Contents lists available at ScienceDirect

Applied Surface Science

journal homepage: www.elsevier.com/locate/apsusc

Permanent superhydrophobic polypropylene nanocomposite coatings by a simple one-step dipping process

Cintia B. Contreras[a], Gabriela Chagas[b], Miriam C. Strumia[a,**], Daniel E. Weibel[b,*]

[a] IMBIV-CONICET, Departamento de Química Orgánica, Facultad de Ciencias Químicas, Universidad Nacional de Córdoba, Haya de la Torre y Medina Allende, Edificio de Ciencias II, Ciudad Universitaria, Córdoba 5000, Argentina
[b] Laboratório de Fotoquímica e Superfícies, Departamento de Físico-Química, Instituto de Química, UFRGS, Av. Bento Gonçalves, 9500, Bairro Agronomia, CEP: 91501-970, CP 15003 Porto Alegre, RS, Brazil

ARTICLE INFO

Article history:
Received 4 February 2014
Received in revised form 1 April 2014
Accepted 2 April 2014
Available online 13 April 2014

Keywords:
Superhydrophobicity
Nanostructuration
Contact angle hysteresis
Titanium dioxide
Coating

ABSTRACT

Superhydrophobic nanocomposite coatings on injection-molded polypropylene (PP) samples were prepared by dipping in xylene solvent containing titanium dioxide nanoparticles (NPs) functionalized with trimethoxypropyl silane. Alternatively, PP samples were dipped in a mixture of functionalized NPs and dissolved PP pellets. As a general result, dip-coated PP samples reached a permanent superhydrophobic state with a contact angle hysteresis (CAH) depending on NPs concentration and surface chemistry. SEM and profilometer measurements show a general trend in the decrease of CAH with the increase of aggregates and roughness. However some results showed that surfaces with the same roughness presented different CAHs. XPS measurements showed that low CAHs and self-cleaning properties were obtained only when the Ti–OH relative concentration on the surface was about 20%. At higher Ti–OH relative concentrations, the surface kept a superhydrophobic static state but lost its self-cleaning properties. This work highlights the fact that both control of the roughness together with chemical surface composition of polar groups have to be taken into account for a precise tuning on the superhydrophobic dynamic component of the surface.

1. Introduction

The control of the wettability of solid surfaces is drawing increasing interest from both theoretical and practical approaches. Wettability is directly related to surface energy and is one of the primary surface properties of solid materials; it is mainly governed by chemical composition and microstructure. Over the last decade, the importance of the nanostructure superimposed on micrometer-scale topology in nature surfaces has been demonstrated [1]. Similarly, artificial superhydrophobic surfaces have been developed on the basis of the lotus leaf or several other natural examples [2–5], such as *Cicada orni*'s wings [3,6] and water strider's legs [7]. Those naturally produced surfaces are water repellent: water droplet rolls off the surface and simultaneously removes its contaminants (self-cleaning effect). The control of surface wettability is crucial in many practical applications, such as thin film technology, lubrication, antifouling paints, self-cleaning windows, microfluids, textiles and anti-snow-sticking surfaces. In recent years, extensive experimental and theoretical research has been devoted to the so-called superhydrophobic surfaces, those that exhibit high water contact angles (WCA) (>150°) and low contact angle hysteresis (CAH) (drops roll off easily even at small inclinations) [3,8–11].

On the basis of two theoretical models mainly, Wenzel's [12] and Cassie-Baxter's [13], numerous methods have been recently used to prepare controlled rough surfaces [2,14]: wet chemical reaction, hydrothermal reaction, electrochemical deposition, self-assembly layer-by-layer, plasma etching, chemical vapor deposition, sol–gel and polymerization reactions. For example, plasma etching processes coupled to chemical coating have demonstrated to be useful to produce superhydrophobic surfaces [10,15–18]. WCA > 170° were obtained using C_4F_8 [15,16] as a gas precursor. Chemical etching has also been used to obtain superhydrophobic surfaces on metals such as copper (154°) [19] or alumina (165°) [20]. Those methodologies usually produced surface roughness in a non-controllable way and new approaches to the problem were developed seeking to control the shape, distribution and

* Corresponding author at: Universidade Federal de Rio Grande do Sul (UFRGS), Físico-Química, Instituto de Química, Avenida Bento Gonçalves, 9500, Bairro Agronomia, 91501-970 Porto Alegre, RS, Brazil. Tel.: +55 5133086204.
** Corresponding author. Tel.: +543515353860.
E-mail addresses: mcs@fcq.unc.edu.ar (M.C. Strumia), danielw@iq.ufrgs.br, danielweibel@yahoo.co.uk (D.E. Weibel).

http://dx.doi.org/10.1016/j.apsusc.2014.04.019
0169-4332/

periodicity of surface topography in the micro scale. By dicing [21] or laser photolithography [8] several hydrophobic micro structures were prepared; experimental results were compared with those of Wenzel–Cassie models. Superhydrophobic alumina films have been successfully developed on industrial aluminum foils by a simple anodization method following by chemical surface modification [22,23].

Most of the above mentioned approaches usually involve many steps or intricate processes that cannot be directly applied to polymers. Polymer materials are widely used in many segments of the industry; its uses and features are defined by characteristics that the material offers, along with its surface. Coating is a crucial step in adjusting the surface properties of the materials including polymers. In this sense, alternative methods to prepare superhydrophobic surfaces on commodities polymers have been recently reported [24–30]. Many polymers present hydrophobic surface properties; however, they are not superhydrophobic and, in contrast to hard materials, such as metals or ceramics, after surface modification they suffer from hydrophobic recovery by regaining their original wettability. For instance, this thermodynamic effect in polypropylene (PP) films is well known when surfaces are modified to hydrophilic properties. PP surfaces modified by different types of plasma treatment show hydrophobic recovery within few days or weeks [31–34]. In polyolefin surfaces, a likely mechanism of hydrophobic recovery is the rotational and/or translational motion of polymer chains and chain segments [32]. These mechanisms determine the observed "loss" of functional groups within the first few monolayers of the surface and lead to a decrease in surface energy. Those thermodynamic processes also take place when hydrophobic groups are grafted into polymer surfaces; alternative methodologies are then used to generate permanent morphology on the surface and increase hydrophobicity [15,35].

Polymeric materials are substituting metals, ceramics and glasses; new applications for superhydrophobic polymers are expected in fields such as antifouling or foul-release coatings, non-wetting textiles, non-icing or ice repellant surfaces, self-cleaning solar cell coatings, among others [2,4,5]. Polymer coating is a very well established method to obtain new surface properties in polymeric materials and recent reports on the preparation of superhydrophobic polymeric substrates using diverse methodologies show the progress in the preparation of self-cleaning polymer surfaces [24,25,36–38]. In particular, polyolefins have broad industrial applications ranging from packaging to building materials and automotive parts and they are widely used where hydrophobicity and clean surfaces are required. A growing interest in converting their hydrophobic surfaces into superhydrophobic ones has also recently developed [39–44]. For instance, Rioboo et al. [41] prepared superhydrophobic PP surfaces by casting or dip-coating solutions of PP of various molecular weight and tacticity. They have investigated the superhydrophobic behavior in terms of initial film thickness and initial solution concentration. Hydrophobic surfaces were obtained at low film thickness. By increasing polymer concentration and, consequently, film thickness, the transition between hydrophobic and superhydrophobic surface is induced.

In this study, we developed a simple one-step dip-nanocomposite coating method to produce PP superhydrophobic films. For the nanocomposite coating, commercial titanium dioxide (TiO_2) nanoparticles (NPs) were first functionalized with trimethoxypropyl silane (TMPSi). Then injection-molded PP samples were simply immersed for a few seconds in hot xylene solutions containing dissolved functionalized TiO_2 NPs or a mixture of dissolved PP together with functionalized TiO_2 NPs. With this approach superhydrophobic surfaces with static water contact angles greater than 160° and very low contact angle hysteresis of less than 5° were produced. The surface properties of the films were characterized by profilometer measurements, scanning electron microscopy (SEM), Fourier transformed infrared spectroscopy in attenuated total reflectance mode (FTIR-ATR) and X-ray photoelectron spectroscopy (XPS) analyses. The wetting property of the coating surface was determined by static and dynamic contact angle measurements.

2. Materials and methods

2.1. Materials

Polypropylene (PP) samples (Braskem S/A, 3.5 g/10 min) were injection-molded, washed ultrasonically with acetone for 30 min, dried at room temperature and then stored in a desiccator. The final PP substrates were about 30 × 10 mm size and 3 mm thickness. Trimethoxypropyl silane (TMPSi) of 97% purity was obtained from Aldrich. Xylene (mixture of isomers) was purchased from Merck (Brazil). Titanium dioxide nanoparticle powder, AEROXIDE® TiO_2-P25, was received from Degussa Corporation and used without any further treatment.

2.2. Production of PP-coated surfaces

TiO_2 NPs functionalization was carried out following the procedure previously published [45]. Briefly, TMPSi in xylene as solvent (5/95 v/v) was prepared by premixing TMPSi and xylene. TMPSi–xylene solution was then stirred for few minutes with a few grams of titanium dioxide.

Two methods were used to produce the superhydrophobic coatings on PP films (see Scheme 1):

(i) Series PPX, NPs–xylene

A varied quantity of NPs was dispersed in 20 mL of the TMPSi–xylene solution and sonicated for 3 h. The temperature of the solution was then increased to 125 °C and a PP stick was immersed. Finally, the stick was removed from the solution and dried in an oven at 100 °C. Different immersion times were studied: the stick was immersed and immediately removed after ~2 s, 3 or 5 s. The NPs concentration in the TMPSi–xylene solution assayed was 0.15, 1.5 and 10% w/v.

(ii) Series PPX-PP, NPs–xylene–PP

In this case, we followed the methodology used in the series (i) with the only difference that 0.3 g of PP pellets were dissolved in the NPs–TMPSi–xylene solution. Different immersion times were studied: the stick was immersed and immediately removed after ~2 s, 3 or 5 s. The NPs concentration in the TMPSi–xylene solution assayed was 0.15, 1.5 and 10% w/v.

Reference PP samples without NPs coatings were also prepared by dipping the PP sticks in xylene solutions following the methodology explained in series (i) and (ii) above.

2.3. Water contact angle measurements

Static water contact angle (WCA) was measured at ambient temperature using a drop of deionized water (4 μL) by gently depositing it on the substrate using a micro syringe. The images were captured using the "Drop Shape Analysis System" equipment, Kruss DSA 30. For each concentration and time, three different modified sticks were studied and all the measurements were repeated at least five times at different positions. For contact angle hysteresis (CAH), the advancing and receding contact angles were measured at the front and back of the droplet moving along the tilted surface, respectively. The tilting angle measurements were performed using a mechanical level goniometer. The images were captured using a digital video camera and analyzed for contact angle measurements using Surftens 3.0 or Image j software.

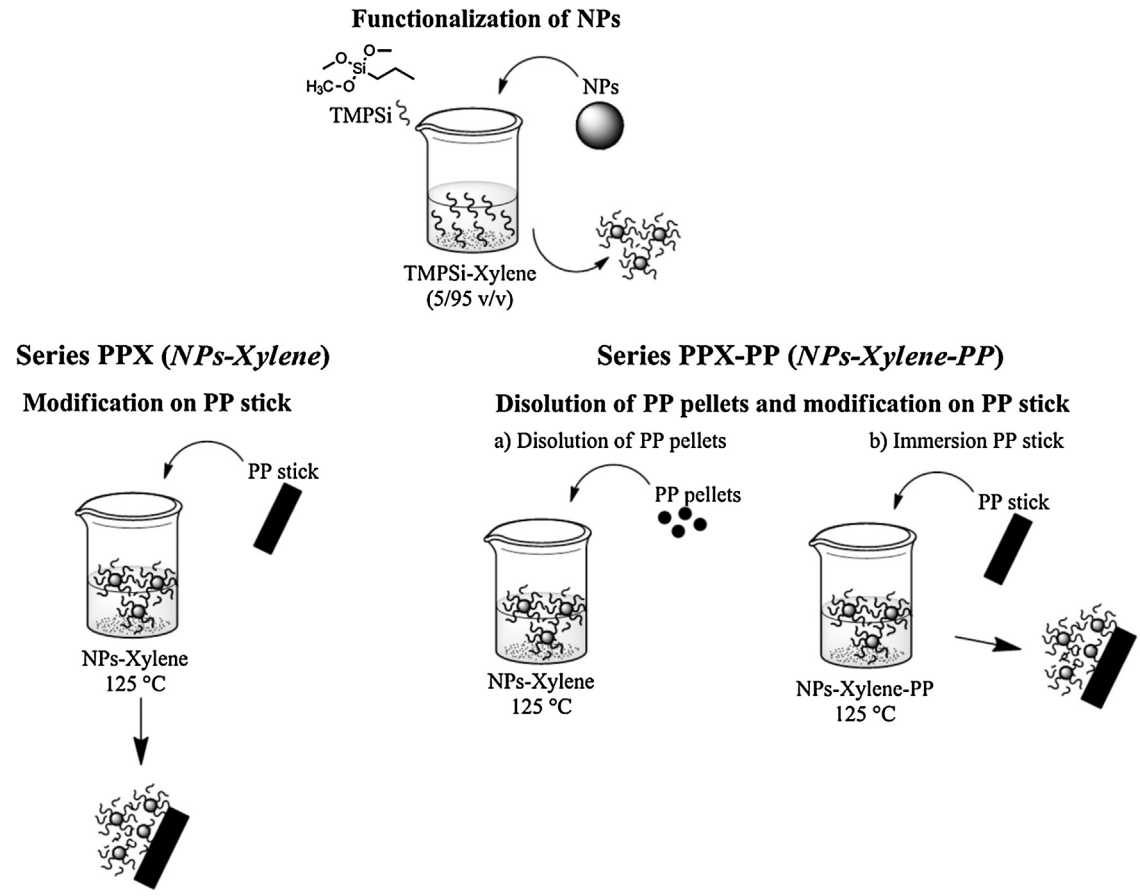

Scheme 1. Two methodologies used for obtaining superhydrophobic polypropylene samples.

2.4. Characterization of the surface morphology

The surface morphologies of the films were mainly observed under scanning electron microscopy, SEM, (Jeol JSM 6060) using an electron acceleration between 5 and 10 kV. Profilometer measurements were carried out by using a profilometer Ambios XP-2 with a stylus of 2.5 mm radius. The arithmetic mean of the surface roughness (Ra) was calculated from the roughness profile; RMS (root mean squared) roughness was finally used.

2.5. Fourier transformed infrared spectroscopy in attenuated total reflectance mode (FTIR-ATR)

FTIR-ATR (Alpha-P model, Bruker) spectra of the casted films were obtained with spectral resolution of 4 cm^{-1}.

2.6. X-ray photoelectron spectroscopy (XPS)

XPS spectra were obtained in a conventional electron spectrometer (Omicron) equipped with a high performance hemispherical energy analyzer with a seven-channeltron detector and using mainly Al $K\alpha$ radiation as the excitation source. Survey spectra were recorded with pass energy of 50 eV, whereas selected atomic signals were acquired with pass energy of 10 eV. In the spectra, the position of the C—C/C—H was specified, and other peaks of different carbon environments were fixed in relation to this peak, set at 285.0 eV. The C 1s envelope was analyzed and peak-fitted after subtraction of a Shirley background using Gaussian–Lorenzian peak shapes obtained from the CasaXPS software package.

3. Results and discussions

Untreated PP films showed a WCA of about 110°. Their wettability behavior after treatment was investigated by WCA measurements. Reference PP samples immersed in xylene at 135 °C for a few seconds and then dried in an oven at 100 °C showed WCAs between (160 ± 2) and (145 ± 3) degrees. SEM images of untreated PP sticks immersed in xylene at 135 °C showed the presence of a microstructure that is not observed in PP without xylene dipping (see Fig. S1 in Supporting information). The increase in roughness of the dipped PP samples explains the increase in the observed WCA. Additionally, the treated pure-PP sticks showed large variation in WCA. The highest WCA values were measured in the central area of the stick and the lowest ones in its borders. In particular the bottom of the stick which remained more time in contact with the xylene solution did not show superhydrophobic properties. In addition, the CAH of the treated samples was always higher than 30° even for the highest WCA measured. Finally, if pure PP samples after treatment were left in a desiccator for about two months, they recovered the WCA of untreated PP sticks (~110°).

Trying to obtain a more homogeneous, permanent superhydrophobic treatment and produce self-cleaning PP sticks, a series of nanocoating on the sticks was carried out. Scheme 1 shows the treatments of PP sticks in xylene solutions containing TiO_2 functionalized NPs (PPX and PPX-PP series). In the PPX series, the WCA measurements for ~2 s of immersion time showed that the increase in NPs concentration produced an increase in WCA, since WCA were (141 ± 7), (160 ± 7) and (164 ± 7) degrees, for NPs concentrations of 0.15, 1.5 and 10% w/v, respectively (see Fig. 1). However, for PPX-PP series, superhydrophobic coatings were obtained from the lowest NPs concentration used (see Fig. 2). The WCA obtained

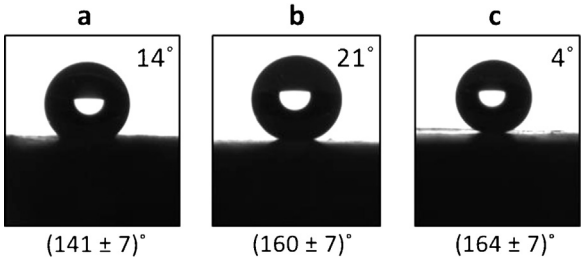

Fig. 1. Images of static water contact angle of PP films dip-coated with functionalized TiO_2 NPs in xylene solutions (PPX series) with ~2 s of immersion time for different NPs concentrations (% w/v): 0.15 (a), 1.5 (b) and 10 (c). The inset in each image shows the contact angle hysteresis of the coated PP films.

were (150 ± 4), (159 ± 6) and (160 ± 3) degrees for NPs concentrations of 0.15, 1.5 and 10% w/v, respectively. When the immersion time increased, a decrease in WCA was observed for both series (see Fig. S1 in Supporting information). If the immersion time increases, a higher degree of dissolution of the top layers of the sticks is found. As a consequence, a lower amount of functionalized TiO_2 NPs adsorbed on the surface should be expected.

The insets of Figs. 1 and 2 show the obtained results on the dynamic properties (CAH) of the dip-coated samples. PPX series showed high hysteresis except for 10% w/v NPs concentration where self-cleaning conditions (low hysteresis) were obtained. By contrast, PPX-PP series presented very low hysteresis with self-cleaning properties, excluding only the lowest concentration of NPs used (0.15% w/v).

To understand the effect of NPs concentration and immersion time on superhydrophobic properties, surface morphology was investigated by SEM and profilometry. SEM images are given in Fig. 3 and roughness results are shown in Fig. 4. From SEM images, it can be seen that the surface of dip-coated PPX or PPX-PP (Fig. 3) has heterogeneous rough surfaces with hierarchical micro- and nano-structures. The TiO_2 nanoparticles were nanometer in dimension (20–29 nm) and their micro–nano aggregates were beneficial for the formation of superhydrophobic surface. SEM images reveal an apparent different surface morphology in PPX and PPX-PP surfaces with varying sizes of hierarchical micro- and nano-structures. The superhydrophobicity of PP surfaces is the result of the evaporation rate of the solvent which depends on the temperature and physical characteristics of the polymer. Additionally, the reorganization process of polymer molecules and their crystallization process during solvent evaporation is a function of the tacticity and molecular weight of the polymer [41,43]. It should be expected that the above dynamic process would be different for PP films dip-coated with functionalized TiO_2 NPs in xylene solution and dip-coated with functionalized TiO_2 NPs in xylene solution also containing dissolved PP pellets, because the composition of the solutions is different.

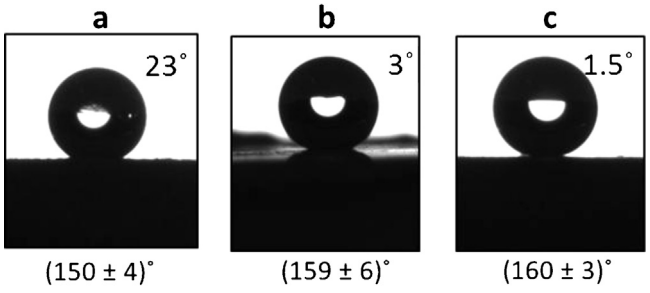

Fig. 2. Images of static water contact angle of PP films dip-coated with functionalized TiO_2 NPs in xylene solutions containing dissolved PP pellets (PPX-PP series) with ~2 s of immersion for different NPs concentrations (% w/v): 0.15 (a), 1.5 (b) and 10 (c). The inset in each image shows the contact angle hysteresis of the coated PP films.

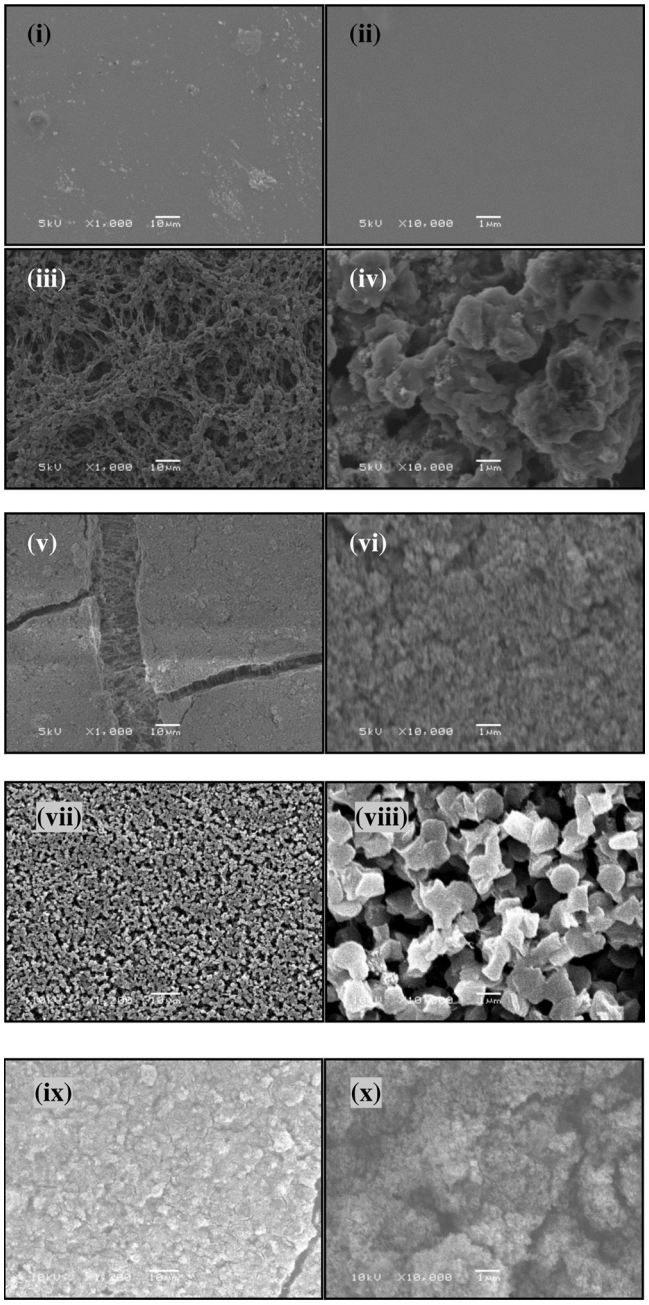

Fig. 3. SEM images of PP films untreated (i–ii); dip-coated with functionalized TiO_2 NPs (0.15% (iii–iv) and 10% (v–vi) (% w/v)) in xylene solution and dip-coated with functionalized TiO_2 NPs (0.15% (vii–viii) and 10% (ix–x) (%w/v)) in xylene solution also containing dissolved PP pellets, all within 2 s of immersion.

Fig. 3(iii–vi) and (vii–x) shows the different morphologies of the final superhydrophobic PP surfaces obtained as a result of the evaporation conditions used in the present work for PPX and PPX-PP series, respectively.

Interestingly, dip-coated PP sticks in solutions with low NPs concentrations (0.15% w/v) for PPX and PPX-PP films showed different types of morphologies with more open regions than PP sticks dipped in solutions containing higher NPs concentrations (see Fig. 3). The high roughness of the samples prepared by dipping in 0.15% w/v NPs concentrations (see Fig. 4) may be due to the open morphology observed in SEM images. Despite this high roughness, almost similar to those of PPX and PPX-PP films, the hysteresis of both films is high, showing no self-cleaning conditions.

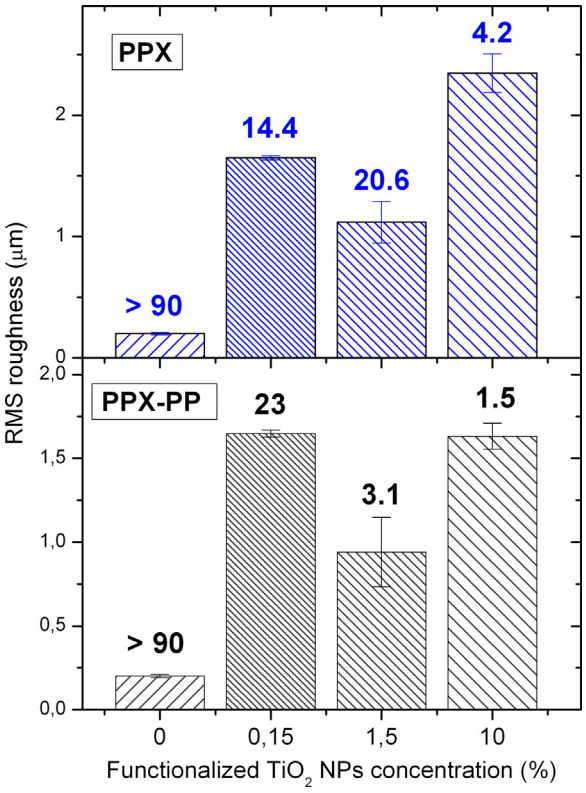

Fig. 4. Roughness data as a function of TiO_2 NPs of PP films dip-coated with functionalized TiO_2 NPs in xylene solution (PPX) and xylene solution also containing dissolved PP pellets (PPX-PP). Immersion time: ~2 s. The numbers on top of the bars represent the contact angle hysteresis of the samples.

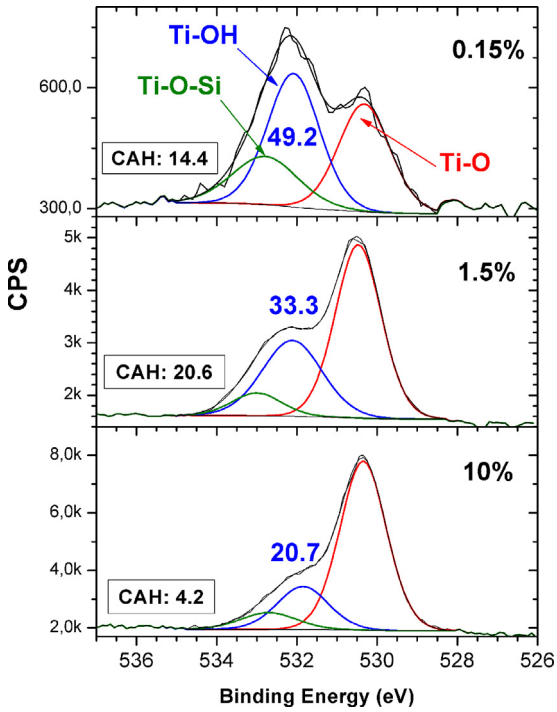

Fig. 5. Core lever O 1s XPS spectra of casted PP films dipped in functionalized TiO_2 NPs dissolved in xylene solution (PPX series) for different NPs concentrations (% w/v): 0.15, 1.5 and 10. Immersion time: ~2 s. The number on the Ti–OH signal represents the relative contribution of this signal to the total spectrum. CAH: contact angle hysteresis.

Fig. 4 shows the profilometer measurements of PPX and PPX-PP prepared films. The RMS roughness increased from $(0.20 \pm 0.01)\,\mu m$ for untreated PP to $(2.3 \pm 0.2)\,\mu m$ and $(1.63 \pm 0.08)\,\mu m$ when the concentration of TiO_2 NPs was 10% w/v in PPX and PPX-PP films, respectively. As a general trend it can be seen that the roughness of the films increased as TiO_2 NPs concentrations increased.

Very low CAH were observed for samples prepared by dipping in solutions containing 10% w/v of NPs independent of the method (PPX or PPX-PP). The data of Fig. 4 also show that RMS of PPX-PP films prepared with solutions containing 0.15 and 10% w/v of NPs were almost the same; however, CAH were very different. The CAH of PPX-PP with 0.15% w/v of NPs was 23° and the CAH of PPX-PP with 10% w/v of NPs was 1.5°. More interestingly, when the concentration of NPs was 1.5% w/v, PPX films showed high hysteresis (20.6°); yet PPX-PP showed very low hysteresis (3.1°). Additionally, Fig. 4 shows that the RMS of both samples is very similar. As a result of the morphology study (SEM and profilometer), the explanation of the differences found in CAH of the prepared superhydrophobic PP samples has to be chemical in origin.

Recent works carried out in our laboratory on superhydrophobic surfaces have arrived to the conclusion that chemical heterogeneity of the surface is highly important in determining contact-angle hysteresis [45–47]. In an attempt to understand the differences in the dynamic component of the superhydrophobic surfaces prepared, surface chemical composition data were obtained by FTIR-ATR and XPS measurements. FTIR-ATR bands confirmed the presence of TMPSi–NPs on the modified surface of the PP sticks for the PPX and PPX-PP series (see Fig. S3 in Supporting information). This was confirmed by the broad intensity band from 700 cm^{-1} corresponding to Ti—O—Ti stretching of titanium dioxide, while the 1129 and 1041 cm^{-1} bands were assigned to stretching vibration of Si—O—Si and Si—O—Si bonding [48,49].

XPS, a very surface-sensitive technique, was used to probe in detail the chemistry at the surface. XPS survey spectra of unmodified and dip-coated PP films were obtained; Table 1 summarizes the results. The elemental composition of the surface of untreated PP, PPX and PPX-PP series were calculated from the relative areas of the XPS signals. The signals of O 1s, Ti 2p, C 1s and Si 2p also confirmed the presence of functionalized TiO_2 NPs with TMPSi on the modified surface of the sticks. An increase in NPs concentration led to an increase in atomic percentage of Ti 2p, O 1s, Si 2p and a decrease in the atomic percentage of C 1s signals of the surfaces studied. To gain insights into the difference in the hysteresis of the coatings, we analyzed the atomic ratio composition in both series of coatings; however, we found no important difference between them (see Table S1 in Supporting information). To clarify the reason of the different hysteresis obtained on the functionalized nanocoatings, O 1s core-level spectra of PP nanocoatings were obtained and analyzed (see Figs. 5 and 6). The O 1s spectra of all the surfaces have three components centered at binding energies

Table 1
Quantification of the elemental contributions by XPS measurements on PP films untreated, dip-coated with functionalized TiO_2 NPs in xylene solution (PPX) and dip-coated with functionalized TiO_2 NPs in xylene solution also containing dissolved PP pellets (PPX-PP). Immersion time: ~2 s.

Sample	TiO_2 NPs concentration (% w/v)	Elemental composition (%)			
		Ti 2p	O 1s	C 1s	Si 2p
Untreated PP		–	2.6	97.4	–
PPX	0.15	1.4	8.4	84.7	5.5
	1.5	7.0	24.2	62.9	5.9
	10	15.1	43.0	33.7	8.2
PPX-PP	0.15	1.4	11.8	79.4	7.4
	1.5	6.2	18.5	71.5	3.8
	10	15.1	43.7	31.6	9.6

Table 2
Summary of the most relevant results for PPX and PPX-PP series (immersion time: 2 s).

Sample	TiO_2 NPs concentration (% w/v)	WCA (°)	CAH (°)	RMS roughness (μm)	Ti–OH concentration (%)
Untreated PP		110		(0.2 ± 0.01)	
PPX	0.15	(141 ± 7)	14.4	(1.65 ± 0.03)	49.2
	1.5	(160 ± 7)	20.6	(1.1 ± 0.3)	33.3
	10	(164 ± 7)	4.2	(2.3 ± 0.2)	20.1
PPX-PP	0.15	(150 ± 4)	23	(1.64 ± 0.04)	51.7
	1.5	(159 ± 6)	3.1	(0.95 ± 0.7)	22.3
	10	(160 ± 3)	1.5	(1.63 ± 0.08)	20.1

of about 530.5, 532.0 and 532.8 eV corresponding to Ti—O, Ti—OH and Ti—O—Si groups. This is in good agreement with the literature values reported [50–52]. The characteristic feature of high hysteresis properties on the nanocoatings in both series (PPX and PPX-PP) involves a sharp increase in the Ti–OH signal centered at 532.0 eV. From Figs. 5 and 6 it is possible to correlate the high CAH of the coatings with a high relative Ti–OH concentration. When the relative Ti–OH intensity signal was higher than about 25%, the prepared PP nanocoating showed high hysteresis. The effect of the hydroxyl groups at the surface is clearly seen when comparing PPX and PPX-PP with 1.5% w/v of functionalized NPs. In both cases the RMSs are quite similar (see Fig. 4); yet, the hysteresis values are very different. A PPX-PP film presents self-cleaning properties (CAH = 3.1°), whereas a PPX film shows high hysteresis (20.6°). The increase in intensity of Ti—OH contributions on the surfaces increases water droplet adhesion, increasing hysteresis. In the PPX-PP method, PP pellets are dissolved together with the functionalized TiO_2 NPs in xylene previous to stick dipping. This can produce an additional extra coating by the same polymer, decreasing the hydroxyl group concentration on the surface region.

Table 2 summarizes the most relevant results for both series studied (PPX and PPX-PP). PP samples dip-coated in solutions containing the two lowest NPs concentrations mainly reached a superhydrophobic state with high hysteresis. By contrast, when the injection-molded PP samples were immersed in solutions containing the highest NPs concentrations studied, surfaces with self-cleaning conditions were obtained.

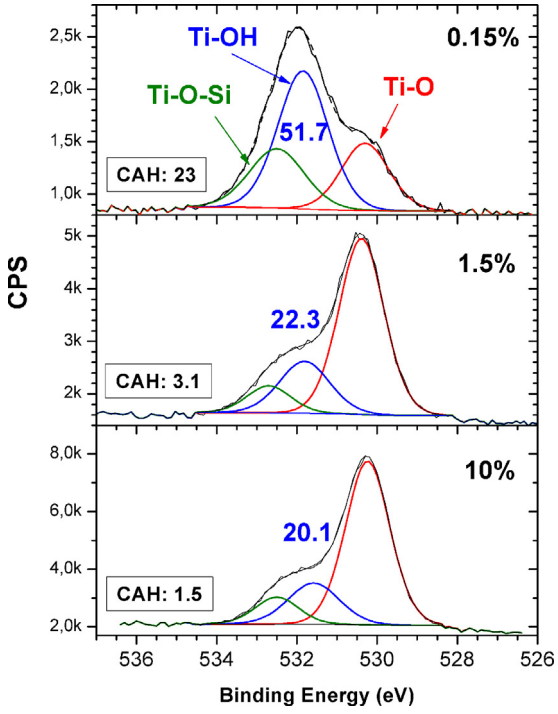

Fig. 6. Core lever O 1s XPS spectra of casted PP films dipped in functionalized TiO_2 NPs dissolved in xylene solution containing dissolved PP pellets (PPX-PP series) for different NPs concentrations (% w/v): 0.15, 1.5 and 10. Immersion time: 2 s. The number on the Ti–OH signal represents the relative contribution of this signal to the total spectrum. CAH: contact angle hysteresis.

Bhushan et al. have recently carried out an experimental and theoretical study of the wetting properties of patterned Si surfaces with cylindrical flat-top pillars of various sizes and pitch distances [53]. For patterned surfaces, they introduced a non-dimensional parameter, the spacing factor (S_f), defined as a ratio between the diameter of the pillars (D) and the pitch distance between them (P). By decreasing the S_f, the values of WCA = 170° and CAH = 5° were achieved. They obtained a good correlation between the CAH measured experimentally and the calculated theoretical values of the CAH as a function of the S_f. The calculations were based on the assumption that the adhesion hysteresis between the solid and the liquid and the density of the pillar edges are the main contribution to the CAH. According to the authors, adhesion hysteresis is a difference in the work of adhesion at the separation of solid and liquid surfaces and the energy gained when bringing them together. They concluded that the WCA, as well as the CAH, depends upon the non-dimensional S_f and both parameters were found independent of the actual size of roughness. The results presented by Bhushan et al. are self-consistent because their substrates (single-crystal silicon) were very homogeneous from the point of view of morphology (the pillars were fabricated using photolithography) and surface chemistry (they were made hydrophobic by coating with a self-assembled 1,1,2,2-tetrahydroperfluorodecyltrichlorosilane monolayer). In our experiments it was found that similar surface roughness has different CAHs (see Table 2). Despite this, it is very difficult to quantify the S_f of our substrates due to non uniform surface morphology; the surface chemistry proved by XPS is clearly different. Adhesion hysteresis will be strongly influenced by irregular polar interactions between Ti–OH groups and water molecules. Surfaces with high Ti–OH concentrations will increase the work of adhesion and their CAHs. Our previous chemical studies on superhydrophobic surfaces also showed that the chemical heterogeneity on the surface strongly influences the final dynamic properties of a superhydrophobic surface [22,45–47].

4. Conclusions

The present work reports a very simple method to fabricate/develop permanent superhydrophobic PP surfaces with different liquid–solid adhesion properties. The superhydrophobic surfaces were fabricated using a simple one-step dip-nano composite coating method to produce PP superhydrophobic films. TiO_2 NPs were first functionalized with TMPSi and then injection-molded PP samples were immersed for a few seconds in hot xylene solutions containing dissolved functionalized TiO_2 NPs or a mixture of dissolved PP together with functionalized TiO_2 NPs. PP sticks immersed in pure xylene solution did not show self-cleaning properties and the static superhydrophobic state was completely lost in about a couple of months. By contrast, when PP sticks were dipped in solutions containing functionalized TiO_2 NPs, the superhydrophobic properties remained stable for the maximum period

measured (one year) showing the excellent durability properties of the nanocoatings. Additionally, further investigations on the increase in adhesion properties of the PP nanocoatings by special photochemical treatment will be reported in a future publication. The main results obtained were explained by a combination of roughness and changes in the chemical composition of the surface. However, surfaces with similar RMS showed almost the same superhydrophobic static WCA, but a different dynamic component of superhydrophobicity. Detailed XPS data revealed that the difference in hysteresis is attributed to a different hydroxyl concentration on the surface. As a general conclusion, it was shown that a superhydrophobic surface in the static and dynamic aspect can only be obtained when the relative Ti–OH concentration is lower than about 25%. This low Ti–OH concentration, in addition to proper roughness, will produce a self-cleaning PP nanocoating. Finally, the present methodology can be easily scaled up because the dipping time treatment is only a few seconds.

Acknowledgments

This work was partially supported by the National Council of Technological and Scientific Development (CNPq), process No. 550461/2012-4, CAPES and FAPERGS/CNPq (10/0050-6). We thank Microscopy and Microanalysis Center (CME), UFRGS for SEM analysis. C.B. Contreras thanks SECyT-UNC for the fellowships awarded.

Appendix A. Supplementary data

Supplementary data associated with this article can be found, in the online version, at http://dx.doi.org/10.1016/j.apsusc.2014.04.019.

References

[1] C. Neinhuis, W. Barthlott, Ann. Bot. (London) 79 (1997) 667.
[2] Z. Guo, W. Liu, B.-L. Su, J. Colloid Interface Sci. 353 (2011) 335.
[3] T.L. Sun, L. Feng, X.F. Gao, L. Jiang, Acc. Chem. Res. 38 (2005) 644.
[4] Y.Y. Yan, N. Gao, W. Barthlott, Adv. Colloid Interface Sci. 169 (2011) 80.
[5] Y. Zhang, Y. Chen, L. Shi, J. Li, Z. Guo, J. Mater. Chem. 22 (2012) 799.
[6] W. Lee, M.K. Jin, W.C. Yoo, J.K. Lee, Langmuir 20 (2004) 7665.
[7] X.F. Gao, L. Jiang, Nature 432 (2004) 36.
[8] L. Barbieri, E. Wagner, P. Hoffmann, Langmuir 23 (2007) 1723.
[9] X.-M. Li, D. Reinhoudt, M. Crego-Calama, Chem. Soc. Rev. 36 (2007) 1350–1368.
[10] Y. Kwon, N. Patankar, J. Choi, J. Lee, Langmuir 25 (2009) 6129.
[11] E. Balaur, J.M. Macak, H. Tsuchiya, P. Schmuki, J. Mater. Chem. 15 (2005) 4488.
[12] R.N. Wenzel, Ind. Eng. Chem. 28 (1936) 988.
[13] A.B.D. Cassie, S. Baxter, Trans. Faraday Soc. 40 (1944) 546.
[14] E. Celia, T. Darmanin, E.T. de Givenchy, S. Amigoni, F. Guittard, J. Colloid Interface Sci. 402 (2013) 1.
[15] L.M. Lacroix, M. Lejeune, L. Ceriotti, M. Kormunda, T. Meziani, P. Colpo, F. Rossi, Surf. Sci. 592 (2005) 182.
[16] M. Lejeune, L.M. Lacroix, F. Bretagnol, A. Valsesia, P. Colpo, F. Rossi, Langmuir 22 (2006) 3057.
[17] P. Roach, N.J. Shirtcliffe, M.I. Newton, Soft Matter 4 (2008) 224.
[18] A. Accardo, F. Gentile, F. Mecarini, F. De Angelis, M. Bughammer, E. Di Fabrizio, C. Riekel, Langmuir 26 (2010) 15057.
[19] Z. Guo, J. Fang, L. Wang, W. Liu, Thin Solid Films 515 (2007) 7190.
[20] K. Tadanaga, J. Morinaga, T. Minami, J. Sol–Gel Sci. Technol. 19 (2000) 211.
[21] Z. Yoshimitsu, A. Nakajima, T. Watanabe, K. Hashimoto, Langmuir 18 (2002) 5818.
[22] D.E. Weibel, A.F. Michels, A.F. Feil, L. Amaral, S.R. Teixeira, F. Horowitz, J. Phys. Chem. C 114 (2010) 13219–13225.
[23] Y. Zhang, X. Yu, H. Wu, J. Wu, Appl. Surf. Sci. 258 (2012) 8253.
[24] I. Yilgor, S. Bilgin, M. Isik, E. Yilgor, Polymer 53 (2012) 1180.
[25] R.V. Lakshmi, T. Bharathidasan, P. Bera, B.J. Basu, Surf. Coat. Technol. 206 (2012) 3888.
[26] A. Das, H.T. Hayvaci, M.K. Tiwari, I.S. Bayer, D. Erricolo, C.M. Megaridis, J. Colloid Interface Sci. 353 (2011) 311.
[27] H.-J. Yu, Z.-H. Luo, J. Polym. Sci. Polym. Chem. 48 (2010) 5570.
[28] L.F. Hong, T.R. Pan, J. Microelectromech. Syst. 19 (2010) 246.
[29] G. Saini, K. Sautter, F.E. Hild, J. Pauley, M.R. Linford, J. Vac. Sci. Technol., A 26 (2008) 1224.
[30] X. Kang, W.W. Zi, Z.G. Xu, H.L. Zhang, Appl. Surf. Sci. 253 (2007) 8830.
[31] L. Köhler, S. Scaglione, D. Flori, J. Riga, R. Caudano, Nucl. Instrum. Methods Phys. Res., Sect. B 185 (2001) 267.
[32] F. Truica-Marasescu, P. Jedrzejowski, M.R. Wertheimer, Plasma Processes Polym. 1 (2004) 153.
[33] F. Truica-Marasescu, S. Guimond, P. Jedrzejowski, M.R. Wertheimer, Nucl. Instrum. Methods Phys. Res., Sect. B 236 (2005) 117.
[34] K.N. Pandiyaraj, V. Selvarajan, R.R. Deshmukh, C. Gao, Appl. Surf. Sci. 255 (2009) 3965.
[35] L.L. Cao, A.K. Jones, V.K. Sikka, J.Z. Wu, D. Gao, Langmuir 25 (2009) 12444.
[36] Y. Lee, K.Y. Ju, J.K. Lee, Langmuir 26 (2010) 14103.
[37] T. Darmanin, F. Guittard, J. Am. Chem. Soc. 131 (2009) 7928.
[38] C. Jiang, Y. Zhang, Q. Wang, T. Wang, J. Appl. Polym. Sci. 129 (2013) 2959.
[39] H. Ji, G. Chen, J. Hu, X. Yang, C. Min, Y. Zhao, J. Dispersion Sci. Technol. 34 (2013) 134.
[40] P.C. Thuene, W. Han, W. Ming, H.J.W. Niemantsverdriet, J. Adhes. Sci. Technol. 22 (2008) 353.
[41] R. Rioboo, M. Voue, A. Vaillant, D. Seveno, J. Conti, A.I. Bondar, D.A. Ivanov, J. De Coninck, Langmuir 24 (2008) 9508.
[42] M. Liu, Z. Jia, F. Liu, D. Jia, B. Guo, J. Colloid Interface Sci. 350 (2010) 186.
[43] H.Y. Erbil, A.L. Demirel, Y. Avcı, O. Mert, Science 299 (2003) 1377.
[44] R. Rioboo, B. Delattre, D. Duvivier, A. Vaillant, J. De Coninck, Adv. Colloid Interface Sci. 175 (2012) 1.
[45] R. Rajajeyaganthan, D.E. Weibel, J. Braz. Chem. Soc. 24 (2013) 1041.
[46] R. Rajajeyaganthan, D.E. Weibel, Appl. Surf. Sci. 258 (2012) 7950.
[47] A.F. Feil, D.E. Weibel, R.R. Corsetti, M.D. Pierozan, A.F. Michels, F. Horowitz, L. Amaral, S.r.R. Teixeira, Appl. Mater. Interfaces 3 (2011) 3981.
[48] T.C. Chang, P.T. Liu, Y.S. Mor, S.M. Sze, Y.L. Yang, M.S. Feng, F.M. Pan, B.T. Dai, C.Y. Chang, J. Electrochem. Soc. 146 (1999) 3802.
[49] L.J. Bellamy, The Infra-Red Spectra of Complex Molecules, Chapman and Hall Ltd., London, 1975.
[50] B. Erdem, R.A. Hunsicker, G.W. Simmons, E.D. Sudol, V.L. Dimonie, M.S. El-Aasser, Langmuir 17 (2001) 2664.
[51] E. McCafferty, J.P. Wightman, Surf. Interface Anal. 26 (1998) 549.
[52] G.W. Simmons, B.C. Beard, J. Phys. Chem. 91 (1987) 1143.
[53] B. Bhushan, M. Nosonovsky, Y. Chae Jung, J. R. Soc. Interface 4 (2007) 643.